Lack of Influence of Substrate on Ligand Interaction with the Human Multidrug And Toxin Extruder, MATE1

Authors:

Lucy J Martínez-Guerrero, Mark Morales, Sean Ekins and Stephen H Wright

Laboratories of Origin:

Department of Physiology, College of Medicine, University of Arizona, Tucson, AZ 85724: LJM-G, MM, and SHW. Collaborations in Chemistry: 5616 Hilltop Needmore Road, Fuquay-Varina, NC, 27526, SE.

Running title page:

Substrate-independence of MATE1inhibition

Corresponding Author:

Stephen H. Wright, PhD

Department of Physiology, University of Arizona, Tucson, AZ 85724, Telephone: (520) 626-4253; Fascimile: (520)-626-2383.

E-mail; shwright@u.arizona.edu

Number of text pages:
Number of tables: 2
Number of figures: 10
Number of references: 55
Number of words in Abstract: 213
Number of words in Introduction: 647
Number of words in Discussion: 1541

Non-Standard Abbreviations:

MATE	Multidrug And Toxin Extruder
OCT	Organic Cation Transporter
OC	organic cation
MPP	1-methyl-4-phenylpyridinium
NBD-MTMA	1-methyl-4-phenylpyridinium (MPP) and, (4) the novel fluorescent probe, N,N,N-trimethyl-2-[methyl(7-nitrobenzo[c][1,2,5]oxadiazol-4-yl)amino]ethanaminium
ASP	4–4-dimethylaminostyryl-N-methylpyridinium
NBuPy	N-butylpyridinium,
BMIM	1-methyl-3-butylimidazolium
BMPy	N-butyl-N-methylpyrrolidinium
$C_{u,max}$	maximum, unbound, drug concentration in plasma
DDI	drug-drug interaction
RPT	renal proximal tubule
NCC	NIH Clinical Collection

ABSTRACT

Multidrug And Toxin Extruder 1 (MATE1) plays a central role in mediating renal secretion of organic cations, a structurally diverse collection of compounds that includes ~40% of prescribed drugs. Because inhibition of transport activity of other multidrug transporters, including the organic cation transporter OCT2, is influenced by the structure of the transported substrate, the present study screened over 400 drugs as inhibitors of the MATE1-mediated transport of four structurally distinct organic cation substrates: the commonly used drugs (1) metformin and (2) cimetidine; and two prototypic cationic substrates, (3) 1-methyl-4-phenylpyridinium (MPP) and, (4) the novel fluorescent probe, N,N,N-trimethyl-2-[methyl(7-nitrobenzo[c][1,2,5]oxadiazol-4-yl)amino]ethanaminium (NBD-MTMA). Transport was measured in Chinese hamster ovary cells that stably expressed the human ortholog of MATE1. Comparison of the resulting inhibition profiles revealed no systematic influence of substrate structure on inhibitory efficacy. Similarly, IC_{50} values for 26 structurally diverse compounds revealed no significant influence of substrate structure on the kinetic interaction of inhibitor with MATE1. The IC_{50} data were used to generate 3D quantitative pharmacophores that identified hydrophobic regions, H-bond acceptor sites, and an ionizable (cationic) feature as key determinants for ligand binding to MATE1. In summary, in contrast to the behavior observed with some other multidrug transporters, including OCT2, the results suggest that substrate identity exerts comparatively little influence on ligand interaction with MATE1.

Introduction

The kidney, particularly the proximal tubule, plays the principal role in clearing organic cations (OCs; molecules that carry a net positive charge at physiological pH) from the body (Hagenbuch, 2010). These OCs include approximately 40% of all prescribed and over-the-counter drugs (incl. cimetidine, procainamide, pindolol, and metformin) (Ahlin et al., 2008; Neuhoff et al., 2003). Thus, renal OC secretion is a critical element in the chain of processes that defines the pharmacokinetics of almost half of drugs to which people are exposed.

The secretion of OCs by the kidney is the consequence of two sequential transport processes in the renal proximal tubule (RPT). The first of these is entry of OC from the blood into an RPT cell across the basolateral membrane by a process that involves electrogenic facilitated diffusion. In humans the basolateral element of OC secretion is dominated by the Organic Cation Transporter, OCT2 (Motohashi et al., 2013; Motohashi et al., 2002). The second step in this process involves exit of OC into the tubular filtrate across the apical, or luminal, membrane of RPT cells by a process that uses electroneutral OC/H^+ exchange. In humans the luminal step is dominated by the Multidrug and Toxin Extruders, MATE1 and MATE2/2-K (Motohashi et al., 2013). The presence within the kidney of this common pathway for the secretion of OCs sets the stage for unwanted drug-drug interactions (DDIs) (Lepist and Ray, 2012). The clinical cost of DDIs is substantial and responsible for approximately 1% of hospital admissions (almost 5% in elderly populations) (Becker et al., 2007; U.S.Food and Drug, 2012), so the ability to predict potential DDIs could lead to decreased morbidity and cost savings.

MATE-mediated OC efflux is both the active and rate-limiting element of the secretory process (Pelis and Wright, 2011; Schäli et al., 1983) and has been implicated in several clinically relevant DDIs (Ito et al., 2012; Lepist and Ray, 2012). To date a primary focus of studies of

MATE function has been establishing the interaction of MATE transporters (typically MATE1) with specific structural classes of drugs (e.g., (Lee et al., 2014; Nies et al., 2012; Yonezawa et al., 2006)). The increasing attention given to the clinical impact of unwanted DDIs, and the growing acceptance of the critical role played by MATE1 in renal OC secretion, has led to development of several predictive models of ligand interaction with hMATE1 (Astorga et al., 2012; Wittwer et al., 2013; Xu et al., 2015), each based on assessing profiles of ligand inhibition of MATE1 transport activity. However, little attention has been given to a critical issue relevant to understanding the influence of MATE1 on unwanted DDI: the potential impact of substrate identity on the profile of drug interaction with MATE1. Increasing evidence suggests that the effectiveness of cationic drugs as inhibitors of multidrug transporters can be significantly influenced by the substrate used to monitor transport activity (Belzer et al., 2013; Hacker et al., 2015; Thevenod et al., 2013), which may complicate the interpretation of decision tree-based assays for assessing potential DDIs (Giacomini et al., 2010; Hillgren et al., 2013). However, the extent to which MATE transporters display such behavior is not clear.

In the current study we screened over 400 drugs as inhibitors of the MATE1-mediated transport of four structurally distinct organic cation substrates: the commonly used drugs (1) metformin and (2) cimetidine; and two prototypic cationic substrate, (3) 1-methyl-4-phenylpyridinium (MPP), and (4) the novel fluorescent probe, N,N,N-trimethyl-2-[methyl(7-nitrobenzo[c][1,2,5]oxadiazol-4-yl)amino]ethanaminium (NBD-MTMA). With the information gained from these screens, plus IC_{50} values determined for a structurally diverse subset of these compounds, we generated machine learning and pharmacophore models, respectively. In contrast to the behavior observed with some other multidrug transporters (Belzer et al., 2013; Ekins et al., 2002b; Garrigues et al., 2002; Hacker et al., 2015; Roth et al., 2011; Westholm et al.,

2009), the results suggest that substrate identity exerts comparatively little, if any, influence on

ligand interaction with MATE1.

Materials and Methods

Chemicals – [^{3}H]1-Methyl-4-phenylpyridinium (MPP) [specific activity (S.A.) 80 Ci/mmol] and [^{3}H]N,N,N-trimethyl-2-[methyl(7-nitrobenzo[c][l,2,5]oxadiazol-4-yl)amino]ethanaminium iodide (NBD-MTMA) [S.A. 85 Ci/mmol] were synthesized by the Department of Chemistry and Biochemistry, University of Arizona (Tucson, AZ). [^{3}H]Cimetidine [S.A. 80 Ci/mmol] was purchased from American Radiochemicals (St Louis, MO), and [^{14}C]metformin [S.A. 107 mCi/mmol] was purchased from Moravek Biochemicals (Brea, CA). Unlabeled cimetidine and metformin were purchased from Sigma-Aldrich Co (St Louis, MO) and AK Scientific, Inc. (Union City, CA), respectively. Unlabeled NBD-MTMA was prepared by the Synthesis Core of the Southwest Environmental Health Sciences Center/Department of Chemistry and Biochemistry of the University of Arizona (Aavula et al., 2006). MPP, Ham's F12 Kaighn's modified medium, and Dulbecco's modified Eagle medium were obtained from Sigma-Aldrich Co. The NIH Clinical Collection (NCC) was acquired from Evotec (So San Francisco, CA). Other reagents were of analytical grade and commercially obtained.

Cell culture and stable expression of transporters – Chinese hamster ovary (CHO) cells containing a single integrated Flp Recombination Target (FRT) site were obtained from Invitrogen (Carlsbad, CA) and were used for stable expression of hMATE1 as previously described (Zhang et al., 2012). Briefly, cells were seeded in a T-75 flask following transfection via electroporation and maintained under selection pressure with hygromycin B (100 μg/ml; Invitrogen). Cells were cultured under 5% CO_2-95% air in a humidified incubator (Nuaire, Plymouth, MN) at 37°C. After two weeks of selection the cells were used for transport studies. Subculture of the cells was performed every 3 to 4 days.

Uptake experiments with cultured cells – CHO cells expressing hMATE1, hOCT2, or wild type control cells, were plated in 96-well cell culture plates (Greiner; VWR Intl., Arlington Heights, IL) at densities sufficient for the cells to reach confluence within 24 hours (50,000 cells per well). For experiments of MATE1 transport activity the cells (MATE1-expressing and control cells) were typically preincubated for 20 min (room temp) in buffer containing 20 mM NH_4Cl (the first step in establishing an outwardly-directed H^+ gradient; (Roos and Boron, 1981)). Plates were then placed in an automatic fluid aspirator/dispenser (Model 406, BioTek, Winooski, VT) and automatically rinsed/aspirated three times with room temperature WB (pH 7.4) and transport was initiated by aspirating this medium and replacing it with 60 µl of an NH_4Cl-free medium (thereby rapidly establishing an outwardly-directed H^+ gradient) containing labeled substrate. Following the experimental incubation the transport reaction was stopped by the rapid (~2 sec) addition (and simultaneous aspiration) of 0.75 ml cold ($4^{o}C$) WB. Following aspiration of the cold stop, 200 µl of scintillation cocktail (Microscint 20, Perkin-Elmer, Waltham, MA) was added to each well and the plates were sealed (Topseal-A; Perkin-Elmer) and allowed to sit for at least 2 hrs before radioactivity was assessed in a 12 channel, multiwell scintillation counter (Wallac Trilux 1450 Microbeta, Perkin-Elmer). Substrate uptake was typically normalized to nominal surface area of confluent cells. For the purpose of comparison to rates reported in studies that normalize transport to cell protein, we find the factor of 0.035 mg cell protein cm^{-2} to be reasonably accurate (Schomig et al., 2006).

Drug screening – The first 5 plates (400 compounds) of the NIH Clinical Collection were used for initial inhibition screening of hMATE1 transport activity. All drugs were diluted using a VIAFLOW electronic, 96 channel pipette (Integra Biosciences, Hudson, NH) to a final concentration of 50 µM in WB at pH 7.4 with 2% DMSO.

Computational modeling – 3D-QSAR pharmacophore generation used Discovery Studio vers 4.1 (Biovia, San Diego, CA). MATE1 IC_{50} values were used as the indicator of biological activity. In this approach (Ekins et al., 2002a), ten hypotheses were generated using hydrophobic, hydrogen bond acceptor, hydrogen bond donor, and the positive and negative ionizable features, and the CAESAR conformer generation method (Li et al., 2007). After assessing all generated hypotheses, the hypothesis with lowest energy cost was selected for further analysis, as this model possessed features representative of all the hypotheses and had the lowest total cost. The total energy cost of the generated pharmacophore was calculated from the deviation between the estimated activity and the observed activity, combined with the complexity of the hypothesis (i.e. the number of pharmacophore features). A null hypothesis, which presumed that there was no relationship between chemical features and biological activity, was also calculated. Therefore, the greater the difference between the energy cost of the generated and null hypotheses, the less likely the generated hypothesis reflects a chance correlation. Also, the quality of the structure-activity correlation between the predicted and observed activity values was estimated via correlation coefficient.

We also generated and validated Laplacian-corrected naïve Bayesian classifier models using Discovery Studio. AlogP, molecular weight, number of rotatable bonds, number of rings, number of aromatic rings, number of hydrogen bond acceptors, number of hydrogen bond donors, and molecular fractional polar surface area and the molecular function class fingerprints of maximum diameter 6 (FCFP_6) were used as the molecular descriptors. Compounds that reduced transport to <10% of control were classed as actives and everything else as inactive. Computational models were validated using leave-one-out cross-validation, in which each sample was left out one at a time, a model was built using the remaining samples, and that model

was used to predict the left-out sample. Each model was internally validated, receiver operator characteristic curve (ROC) plots were generated, and the cross-validated receiver operator characteristic curve's area under the curve (XV ROC AUC) was calculated. 5-fold cross validation (leave out 20% of the dataset, and repeat 5 times) was also performed. Bayesian Models were also built with the FCFP6 descriptor only using CDD Models in the CDD Vault (Clark et al., 2015; Clark and Ekins, 2015) and 3-fold cross validation performed.

Data analysis – Results are presented as means ±SE. Unless otherwise noted, statistical analyses were performed using a two-tailed unpaired Student's t-test. In some cases data sets were compared using 1- or 2-way ANOVA (with Bonferroni post tests). Curve-fitting used algorithms found in Prism 5.03 (GraphPad Software Inc, San Diego, CA).

Results

Kinetic characterization of MATE1 transported substrates – Four compounds shown previously

to be substrates of MATE1 were selected for study. Selection criteria included (i) structures that

differed substantially from one another and (ii) rates of transport sufficiently large to permit

accurate kinetic analyses of inhibition. The selected compounds were: [3H]MPP, [3H]NBD-

MTMA, [14C]metformin and [3H]cimetidine. The former two are model substrates for OC

transport research (Aavula et al., 2006; Bednarczyk et al., 2000; Lazaruk and Wright, 1990),

whereas metformin and cimetidine are therapeutic agents in wide use in the U.S and other

countries, both of which are secreted by the renal OCT2-MATE1/2K pathway (Nies et al., 2011).

Figure 1 shows the structures of these substrates with comparisons of similarity, as assessed by

Tanimoto similarity coefficients (Bajusz et al., 2015) (Discovery Studio), emphasizing their

structural diversity.

Figure 2 shows time courses of MATE1 mediated uptake of the four test substrates, each

corrected for uptake into WT CHO cells. Under the condition of the outwardly-directed H^+

gradient used in these experiments uptake of all four substrates was nearly linear for almost 60

seconds, and a 30 second time point was used to provide an estimate of the initial rate of

transport for all substrates in the subsequent experiments. Figure 3 shows the kinetics of

MATE1-mediated transport of the four test substrates. The transport of each was adequately

described by the Michaelis-Menten equation for competitive interaction of labeled and unlabeled

substrate as described previously (Malo and Berteloot, 1991):

$$J^* = \frac{J_{max}[S^*]}{K_{tapp} + [S^*] + [S]} \qquad \text{eq. 1}$$

where J* is the rate of transport of the radiolabeled substrate from a concentration of the labeled

substrate equal to [S*]; J_{max} is the maximal rate of mediated substrate transport; K_{tapp} is the

apparent Michaelis constant of the transported substrate; [S] is the concentration of unlabeled

substrate (note: uptakes at each substrate concentration were corrected for the nonsaturable

component of labeled substrate accumulation that reflected the combined influence of diffusion,

nonspecific binding, and incomplete rinsing of labeled substrate from the cell culture well). The

different substrates exhibited a wide range of kinetic values. The transporter had the highest

apparent affinity, but lowest transport capacity, for cimetidine (K_{tapp} of 2.2 µM and J_{max} of 4.9

pmol cm^2 min^{-1}); and the lowest apparent affinity, but highest capacity, for metformin (K_{tapp} of

336 µM and J_{max} of 344 pmol cm^{-2} min^{-1}). The kinetic parameters for MPP and NBD-MTMA

transport were distributed between these extremes (see Table 1). Transport efficiency (the ratio

of J_{max} to K_{tapp}) provides a comparative measure of 'carrier-mediated permeability' (Schomig et

al., 2006)) varied by a factor of 5, with MPP transport being 'most efficient,' and NBD-MTMA

transport being 'least efficient' (Table 1).

Screening of inhibition of MATE1-mediated transport – Figure 4 shows the inhibitory influence

of each of the four test substrates on transport of the other three. As expected, increasing

concentrations of each compound resulted in increasing inhibition of transport activity. This

inhibition was described by the following relationship:

$$J^* = \frac{J_{app}[S^*]}{IC_{50} + [I]}$$

eq. 2

where J^* is the rate of MATE1-mediated transport of labeled substrate from a concentration of

substrate equal to $[S^*]$ (which was selected to be much less than the K_{tapp} for transport of that

substrate), IC_{50} is the concentration of inhibitor that reduces mediated (i.e., blockable) substrate

transport by 50%, and J_{app} is a constant that includes the maximal rate of substrate transport

times the ratio of the inhibitor IC_{50} and the K_{tapp} for transport of the labeled substrate (Groves et

al., 1994) (note; uptakes at each inhibitor concentration were corrected for uptake measured in wild type CHO cells). If the four test substrates compete with one another for a common binding site, then one may expect that each will have a single IC_{50} value that is equal to its K_{tapp} for transport (Segel, 1975). That proved to be the case; for each compound there was no significant difference between its K_{tapp} value and the IC_{50} values it produced against transport of the other test molecules (Fig. 4 and Table 1).

To assess the influence of inhibitor structure on inhibitory effectiveness we used the National Institutes of Health Clinical Collection (http://www.nihclinicalcollection.com/). Our examination began with a 'low resolution' screen of inhibition of MATE1-mediated transport of the four test substrates produced by a single concentration (50 µM) of each of 400 compounds from the NCC (Supplemental Data File 1). These compounds included a broad array of physicochemical characteristics, including a structurally diverse set of organic 'cations,' organic 'anions,' and neutral compounds, i.e., compounds that carried net positive, negative, or zero charge at physiological pH. Figure 5 shows the profile of inhibition of all the test drugs against MATE1-mediated transport of MPP, NBD-MTMA, cimetidine and metformin (see also Supplemental Data File 1). The order of test agents is the same for each substrate and reflects the order of (top to bottom) increasing inhibition of MPP transport. For the purpose of comparison, compounds were considered to be comparatively 'effective' inhibitors if the 50µM test concentration reduced MATE1-mediated transport by 50% or more. By this criterion about 30% of the test compounds were effective inhibitors (MPP, 34.3%; NBD-MTMA, 32.5%, cimetidine, 25.3%; metformin, 36.3%). Moreover, as shown in the inhibitory profiles presented in Figure 5, the overall profile of inhibition was similar for the four test substrates, though the rank order of effectiveness differed somewhat between the four. The top 30 most effective inhibitors of

transport of each substrate, included 14 compounds in common (alosetron, amisulpride, azaset-

tron, donepezil, 6-([2-(1h-imidazol-4-yl)ethyl]amino)-n-[4-(trifluoromethyl)phenyl]heptanamide

(2z)-2-butenedioate (1:1), lofexidine, midazolam, ormetoprim, perospirone, risperidone,

rosiglitazone, topotecan, tropisetron, ondansetron).   The overall similarity of inhibitory

effectiveness displayed by the NCC compounds is evident in the series of pairwise comparisons

shown in Figure 6, in which the percent inhibition by each test agent is compared for each pair of

substrates, e.g., inhibition of MATE1-mediated MPP transport vs. inhibition of NBD-MTMA

transport (Fig. 6A). For each paired comparison a simple regression of the data is shown (in red),

as well as the 'line of identity' (blue) that depicts equal inhibition of transport of both substrates

by all compounds. The similarity of inhibition profiles between the four substrates is evident.

Furthermore, Bland-Altman analysis provided no support for the presence of significant

systematic differences (fixed bias) in inhibitory profiles between any of the substrate pairs

(Supplemental Figure 1).

Inhibitory profiles of selected compounds – To obtain a more precise understanding of the

structural characteristics associated with inhibition of MATE1-mediated transport of the four test

substrates, a subset of the NCC collection (22 compounds) was selected to determine IC_{50} values.

Principal Component Analysis (PCA) was used to compare the molecular descriptor space

(ALogP, Molecular_Weight, Num_H_Donors, Num_H_Acceptors, Num_RotatableBonds,

Num_Rings, Num_AromaticRings, Molecular_PolarSurfaceArea, FCFP_6) of 80 high affinity

('effective') and 80 modest to low affinity ('ineffective') inhibitors of MATE1 transport.

Supplemental Figure 2 shows 3D PCA plots of 'effective' and 'ineffective' inhibitors of MPP

transport (as determined from the 50 µM screen of the NCC). The yellow symbols show the

distribution within the PCA-defined chemical space of a subset of structurally diverse

'effectives' and 'ineffectives' from which 22 compounds (Supplemental Figure 2C), reflecting a broad range of inhibitory effectiveness, were selected to generate IC_{50} values for inhibition of each test substrate.

To show the range of inhibition of MATE1-mediated transport produced by the broad array of structures used in the 'high resolution' screen, Figure 7 shows an example of 5 structurally distinct drugs that displayed a broad range of inhibitory effectiveness, with IC_{50} values that ranged over three orders of magnitude, from ~ 300 nM (famotidine) to ~300 µM (venlaxafine). Substrate identity had comparatively little effect on IC_{50} values for these five compounds; the IC_{50} values measured against the four test substrates did not vary by more 60% from the average determined for each inhibitor.

The general agreement between IC_{50} values measured against transport of the four test substrates is evident in the pairwise comparisons presented in Figure 8, which compares directly the log of the IC_{50} values for the test inhibitors generated against each substrate with those determined for the other substrates (Table 2). Regression analysis of these log-log relationships revealed that none of the slopes were different from 1 (P>0.05). The average ratio of individual IC_{50} values for each set of comparisons did not vary by more than 30%, and of the 156 individual comparisons only 2 varied by more than 2-fold. These observations show that there was no systematic, i.e., consistent, tendency for the transport of any of the four test substrates to be inhibited with more or less effectiveness by the test inhibitors.

The set of substrates used in the current study did not include the fluorescent OC, ASP, which has been used as a test substrate to assess selectivity of both OCT2 (Kido et al., 2011) and MATE1 (Wittwer et al., 2013). In the study of MATE1 selectivity Wittwer et al (Wittwer et al., 2013) screened 900+ compounds for inhibition of MATE1-mediated ASP transport and noted, as

discussed below for the present study, that cationic charge and hydrophobicity were positively correlated with inhibition of MATE1 activity. Eighty-six compounds in the set of ligands used in the current study were included in the Wittwer report and Supplemental Figure 3A compares the degree of inhibition of MPP transport reported here with the inhibition of ASP transport reported in that study. There was a clear correlation between the inhibitions produced by this common set of ligands. Although it appeared that, in general, there was a greater degree of inhibition of MPP transport than of ASP transport (particularly evident for the 'higher affinity' inhibitors distributed toward the left side of Supplemental Figure 3A), that probably reflected the use of a 50 µM screening concentration in our study compared to a 20 µM screening concentration in the study by Wittwer et al. (Wittwer et al., 2013). Figure S3B compares for five compounds the IC_{50} values for inhibition of MPP or metformin transport we determined, to the values obtained by Wittwer et al. for inhibition of ASP transport. Within the limits of resolution provided by this small sample, there was little evidence for a systematic variation in IC_{50} values obtained for the two substrates.

Development of MATE1 pharmacophores and Bayesian machine learning models – Figure 9 shows the 3D pharmacophores developed from data on the inhibition produced by the 22 test drugs of the NCC plus the test substrates when used as inhibitors against MATE1-mediate transport of the four test substrates (total = 26 molecules). Each is shown overlaid with the structure of gabexate, which was a particularly good inhibitor of all four substrates. Given the relative independence of substrate-identity on the profile of inhibition evident in Figure 8, it was not unexpected that the four pharmacophores were generally quite similar to one another. Figure 10 shows the observed versus expected IC_{50} values calculated using these pharmacophores (MPP, r = 0.80; NBD-MTMA, r = 0.81; cimetidine, r = 0.81; metformin, r = 0.79). For MPP,

NBD-MTMA and cimetidine, each pharmacophore included two hydrogen bond acceptor features (green), one hydrophobic region (cyan) and an ionizable (i.e., cationic) feature (red). The pharmacophore developed for metformin (Fig. 9D) included only one hydrogen bond acceptor feature, two hydrophobic regions and one ionizable feature, but cluster analysis revealed little or no statistical difference between the pharmacophores, which is evident in the spatial alignment of the four pharmacophores (Fig. 9E).

Six molecules, BMIM (IC$_{50}$ of 178.7 µM), NBuPy (26.5 µM), alosetron (0.1 µM), levofloxacin (51.6 µM), nifekalant (2.9 µM) and terbinafine (1209 µM)), were used as a test set and IC$_{50}$ data were generated for inhibition of MPP transport (predicted vs. measured values are shown in Fig. 10; predictions based on all four pharmacophores are presented in Supplemental Table 1). NBuPy, alosetron and nifekalant were consistently predicted as less potent inhibitors than the measured values revealed. The six compounds were added to the MPP set and this resulted in a model with the same features but a different arrangement (Supplemental Figure 4).

Discussion

'Decision tree-based' predictions of potential DDIs with multidrug transporters are complicated when the quantitative profile of inhibition of transport by a potential perpetrator is influenced by the choice of substrate used to assess transport activity (e.g., (Hacker et al., 2015)). Although increasingly viewed as an issue for OCTs, P-gp and OATPs (Belzer et al., 2013; Garrigues et al., 2002; Hacker et al., 2015; Roth et al., 2011), the extent to which ligand interaction with MATE1 displays a similar substrate-dependence, is not clear. The two screens of inhibitor interaction with MATE1 reported to date focused on profiles generated against transport of single substrates, i.e., MPP (Astorga et al., 2012) or ASP (Wittwer et al., 2013). We did, however, recently report that two structurally distinct 'ionic liquids' (BMIM and BMPy) had IC_{50} values for inhibition of MATE1-mediated transport of $[^3H]$MPP that were about 4-fold lower than the values observed for inhibition of transport of $[^3H]$triethylmonomethylammonium, consistent with the concept of 'substrate-dependent ligand interaction' with MATE transporters (Martinez-Guerrero and Wright, 2013). The current results, however, suggest that substrate identity exerts comparatively little influence on ligand interaction with MATE1.

This conclusion was based on the assessment of transport of four structurally diverse MATE1 substrates, two drugs in common clinical use (metformin and cimetidine) and two 'probe' OCs (MPP and NBD-MTMA) (Fig. 1). When tested as inhibitors of each other's transport, there were no significant differences between each substrate's K_{tapp} and the IC_{50} values they displayed against transport of the others (Figs. 3 and 4). Thus, within the limits of this restricted list of compounds, there was no evidence of a substrate-dependence to the interaction of these structurally distinct ligands with MATE1. This was followed by a low resolution screen of 400 compounds from the NCC that provided a broadly based assessment of the influence of

structural diversity on ligand interaction with MATE1. Although the rank order of inhibitory effectiveness varied slightly for the four test substrates (Fig. 5), no systematic differences were noted. In other words, the results of the low resolution screen revealed no indication that transport of one of the test substrates was more efficiently reduced by exposure to inhibitory ligands than any of the other substrates (Figs. 6 and Supplemental Figure 1). Finally, substrate-to-substrate pairwise comparisons of IC_{50} values determined for the structurally diverse subset of the NCC also revealed no differences for the inhibitory interaction of the test compounds against transport of the test substrates (Fig. 8). These data are consistent with the four test substrates and the set of test inhibitors competing for interaction at a common binding site (or a set of mutually exclusive sites) at the external face of the transporter.

The qualifier, "external" face of the transporter, is important. The present observations, indeed those from virtually all studies on MATE transport to date (Wright, 2014), focused on the kinetic characteristics of the transporter operating in an 'uptake' mode. However, in its normal physiological role as the second step in OC secretion, MATE1 mediates efflux of its organic substrates. The emphasis on influx largely reflects the technical challenges associated with accurate assessment of rates of efflux. Cytoplasmic substrate activity is difficult to quantify, and because cells are small, the cytoplasmic substrate concentration during efflux changes very rapidly; the combination of these issues typically confounds efforts to measure the kinetics of efflux. It should be acknowledged that, although there are thermodynamic constraints on the kinetic properties of 'influx' vs. 'efflux', they need not be 'symmetrical' need (Stein, 1990); in other words, under so-called 'zero-trans' conditions, the apparent affinity for substrate (or inhibitor) of the cytoplasmic face of MATE1 need not be the same as that of the extracellular face. Thus, whereas the rank ordering of ligand affinity may be expected to be qualitatively

similar at the two faces of the membrane (e.g., both membrane faces of OCT2 display much higher affinity for tetrabutylammonium and corticosterone than for TEA and choline; (Volk et al., 2003)), the few studies that have made such measurements suggest that the absolute Kt or IC50 values can differ by 10-fold (or more) (Stein, 1990).

The absence of systematic substrate-dependence of ligand inhibition for MATE1 was in rather marked contrast to the evidence for such effects with OCT2. Two studies that examined the influence of substrate on inhibition of OCT2 transport included MPP and metformin as test substrates (Belzer et al., 2013; Hacker et al., 2015). In both studies the test inhibitors exerted a significantly greater inhibition of metformin transport than of MPP transport. These data were cited as being consistent with the view expressed by others (Egenberger et al., 2012; Harper and Wright, 2012; Koepsell, 2011; Zhang et al., 2005) that ligand interaction with OCT transporters may involve interaction at a binding surface that can support binding of two or more ligands at once. The observation here of inhibitor interactions with MATE1 that consistently displayed the same apparent inhibitor constants, regardless of substrate identity, suggest that substrates and inhibitory ligands typically interact at a kinetically common binding site at the external face of MATE1. It is, therefore, interesting to note that crystal structures of the prokaryotic MATE transporter, NorM, bound to three distinct ligands (ethidium, rhodamine 6G, and tetraphenylphosphonium) show these ligands occupying a common binding locus at the external face of the protein (Lu et al., 2013). The authors noted the presence of multiple acidic residues in the binding region that may enable versatile orientation and charge complementation of structurally dissimilar cationic drugs in NorM without the need to revamp the drug binding site. Given its multispecificity, it is intriguing to speculate that a similar strategy may exist for human MATE1.

Common feature 3D pharmacophores for MATE1 were generated previously for inhibition of MATE1-mediated MPP transport and consisted of multiple hydrophobic, hydrogen bonding and positive ionizable features (Astorga et al., 2012). In this study we identified these same features when we generated pharmacophores for the 26 compounds screened as inhibitors of four distinct substrates (Fig. 9) using a quantitative 3D pharmacophore approach. We had also previously used Bayesian machine learning with the MATE1 inhibitor data for 46 molecules (Astorga et al., 2012), which suggested nitrogen-containing heterocycles are positively correlated with MATE1 interaction. In the current study we used the data for 400 compounds screened as inhibitors to generate four models as well as a consensus model and these all showed that nitrogen containing rings were again shown as important for activity while hydroxyl, carboxylic acids and chlorine substitutions were unfavorable for MATE1 inhibition (Supplemental Figure 5). The independent computational approaches using either the complete dataset or a subset of 26 molecules pointed to minimal differences in the models created for each substrate probe. Our human MATE1 models are also in good agreement with those we observed earlier (Astorga et al., 2012). Xu *et al*. (Xu et al., 2015) recently used a combinatorial pharmacophore approach with the data from Witter *et al*. (Wittwer et al., 2013) and described four unique pharmacophores for inhibitors of MATE1. However, our results suggest that one pharmacophore is likely sufficient to explain inhibitory binding to MATE1. But using pharmacophores alone to score compounds fitting to a discrete pharmacophore may not be ideal as we showed using a small test set of six molecules; whereas 3 were reasonably well-predicted (BMIM, levofloxacin, and nifekalant), 3 were not (NBuPy, alosetron, and terbinafine; Supplemental Table 1). Perhaps adding some van der Waals shape restriction to the pharmacophores may help to limit prediction error. An additional approach that uses the full extent of the screening data generated may be a

useful addition also. We recently described how Bayesian models can be generated with open source FCFP6 descriptors and a Bayesian algorithm to enable transporter models to be shared and used in mobile apps (Ekins et al., 2015), and we used the data from Wittwer *et al.* (Wittwer et al., 2013), and our own earlier study (Astorga et al., 2012) as an example. This produced Bayesian models with 5-fold ROC values of 0.65 and 0.75, respectively. When we used the consensus MATE1 dataset in the current study, containing 12 actives across all 4 substrates and the remaining inactives, the 3-fold cross validation was 0.82 using the open FCFP6 descriptor only (Supplemental Figure 5; Supplemental Tables 2 and 3). These AUC values using commercial or open source modeling approaches are comparable to those obtained by Wittwer et al., (Wittwer et al., 2013) and their random forest model for over 800 molecules as inhibitors of ASP. While pharmacophores can produce compelling images that help explain the 3D nature of the ligand-protein interaction, machine learning may be more useful for classifying compounds and their potential for DDI at MATE1.

In conclusion, our experimental and computational data using structurally diverse substrate probes and over 400 diverse molecules tested as potential inhibitors suggest that, unlike the situation with OCT2, the interaction of inhibitory ligands with MATE1 is not systematically influenced by the structure of the substrate used to assess transport activity. Thus, in general, our observations support the conclusion that broad screening for DDIs can use a single substrate, (arguably metformin, given its utility in both *in vitro* and *in vivo* testing) and that ITC/FDA decision trees can be applied without concern for the complicating influence of substrate structure for MATE1.

Authorship Contributions

Participated in research design: LJM-G, SE, and SHW.
Conducted experiments: LJM-G and MM.
Contributed new reagents or analytic tools: none.
Performed data analysis: LJM-G, MM, SE and SHW.
Wrote or contributed to the writing of the manuscript: LJM-G, SE and SHW.

References

Aavula BR, Ali MA, Bednarczyk D, Wright SH and Mash EA (2006) Synthesis and fluorescence

of n , n , n -trimethyl-2-[methyl(7-nitrobenzo[c][1,2,5]oxadiazol-4-yl)amino]ethanaminium

iodide, a pH-insensitive reporter of organic cation transport. *Synthetic Comm* **36**: 701-705.

Ahlin G, Karlsson J, Pedersen JM, Gustavsson L, Larsson R, Matsson P, Norinder U, Bergstrom

CA and Artursson P (2008) Structural requirements for drug inhibition of the liver specific

human Organic Cation Transport protein. *J Med Chem* **51**(19): 5932-5942.

Astorga B, Ekins S, Morales M and Wright SH (2012) Molecular determinants of ligand

selectivity for the human Multidrug And Toxin Extrusion proteins, MATE1 and MATE-2K.

J Pharmacol Exp Ther **341**(3): 743-755.

Bajusz D, Racz A and Heberger K (2015) Why is Tanimoto index an appropriate choice for

fingerprint-based similarity calculations? *J Cheminform* **7**: 20.

Becker ML, Kallewaard M, Caspers PW, Visser LE, Leufkens HG and Stricker BH (2007)

Hospitalisations and emergency department visits due to drug-drug interactions: a literature

review. *Pharmacoepidemiol Drug Saf* **16**(6): 641-651.

Bednarczyk D, Mash EA, Aavula BR and Wright SH (2000) NBD-TMA: a novel fluorescent

substrate of the peritubular organic cation transporter of renal proximal tubules. *Pflugers

Arch* **440**(1): 184-192.

Belzer M, Morales M, Jagadish B, Mash EA and Wright SH (2013) Substrate-dependent ligand

inhibition of the human Organic Cation Transporter, OCT2. *J Pharmacol Exp Ther* **346**: 300-

310.

Clark AM, Dole K, Coulon-Spektor A, McNutt A, Grass G, Freundlich JS, Reynolds RC and

Ekins S (2015) Open Source Bayesian Models. 1. Application to ADME/Tox and Drug

Discovery Datasets. *J Chem Inf Model* **55**(6): 1231-1245.

Clark AM and Ekins S (2015) Open Source Bayesian Models. 2. Mining a "Big Dataset" To

Create and Validate Models with ChEMBL. *J Chem Inf Model* **55**(6): 1246-1260.

Egenberger B, Gorboulev V, Keller T, Gorbunov D, Gottlieb N, Geiger D, Mueller TD and

Koepsell H (2012) A substrate binding hinge domain is critical for transport-related structural

changes of Organic Cation Transporter 1. *J Biol Chem* **287**(37): 31561-31573.

Ekins S, Clark AM and Wright SH (2015) Making Transporter Models for Drug-Drug

Interaction Prediction Mobile. *Drug Metab Dispos* **43**(10): 1642-1645.

Ekins S, Kim RB, Leake BF, Dantzig AH, Schuetz EG, Lan LB, Yasuda K, Shepard RL, Winter

MA, Schuetz JD, Wikel JH and Wrighton SA (2002a) Application of three-dimensional

quantitative structure-activity relationships of P-glycoprotein inhibitors and substrates. *Mol*

Pharmacol **61**(5): 974-981.

Ekins S, Kim RB, Leake BF, Dantzig AH, Schuetz EG, Lan LB, Yasuda K, Shepard RL, Winter

MA, Schuetz JD, Wikel JH and Wrighton SA (2002b) Three-dimensional quantitative

structure-activity relationships of inhibitors of P-glycoprotein. *Mol Pharmacol* **61**(5): 964-

973.

Garrigues A, Loiseau N, Delaforge M, Ferte J, Garrigos M, Andre F and Orlowski S (2002)

Characterization of two pharmacophores on the multidrug transporter P-glycoprotein. *Mol*

Pharmacol **62**(6): 1288-1298.

Giacomini KM, Huang SM, Tweedie DJ, Benet LZ, Brouwer KL, Chu X, Dahlin A, Evers R,

Fischer V, Hillgren KM, Hoffmaster KA, Ishikawa T, Keppler D, Kim RB, Lee CA, Niemi

M, Polli JW, Sugiyama Y, Swaan PW, Ware JA, Wright SH, Wah YS, Zamek-Gliszczynski MJ and Zhang L (2010) Membrane transporters in drug development. *Nature reviews Drug discovery* **9**(3): 215-236.

Groves CE, Evans K, Dantzler WH and Wright SH (1994) Peritubular organic cation transport in isolated rabbit proximal tubules. *Am J Physiol* **266**: F450-F458.

Hacker K, Maas R, Kornhuber J, Fromm MF and Zolk O (2015) Substrate-dependent inhibition of the human Organic Cation Transporter OCT2: A comparison of metformin with experimental substrates. *PLoS One* **10**(9): e0136451.

Hagenbuch B (2010) Drug uptake systems in liver and kidney: a historic perspective. *Clin Pharmacol Ther* **87**(1): 39-47.

Harper JN and Wright SH (2012) Multiple mechanisms of ligand interaction with the human organic cation transporter, OCT2. *Am J Physiol Renal Physiol* **304**(1): F56-F67.

Hillgren KM, Keppler D, Zur AA, Giacomini KM, Stieger B, Cass CE, Zhang L and International Transporter C (2013) Emerging transporters of clinical importance: an update from the International Transporter Consortium. *Clin Pharmacol Ther* **94**(1): 52-63.

Ito S, Kusuhara H, Yokochi M, Toyoshima J, Inoue K, Yuasa H and Sugiyama Y (2012) Competitive inhibition of the luminal efflux by multidrug and toxin extrusions, but not basolateral uptake by organic cation transporter 2, is the likely mechanism underlying the pharmacokinetic drug-drug interactions caused by cimetidine in the kidney. *J Pharmacol Exp Ther* **340**(2): 393-403.

Kido Y, Matsson P and Giacomini KM (2011) Profiling of a prescription drug library for potential renal drug-drug interactions mediated by the organic cation transporter 2. *J Med Chem* **54**(13): 4548-4558.

Koepsell H (2011) Substrate recognition and translocation by polyspecific organic cation transporters. *Biol Chem* **392**(1-2): 95-101.

Lazaruk KDA and Wright SH (1990) MPP$^+$ is transported by the TEA$^+$-H$^+$ exchanger of renal brush-border membrane vesicles. *Am J Physiol* **258**: F597-F605.

Lee JH, Lee JE, Kim Y, Lee H, Jun HJ and Lee SJ (2014) Multidrug and Toxic Compound Extrusion Protein-1 (MATE1/SLC47A1) is a novel flavonoid transporter. *J Agric Food Chem* **62**(40): 9690-9698.

Lepist EI and Ray AS (2012) Renal drug-drug interactions: what we have learned and where we are going. *Expert Opin Drug Metab Toxicol* **8**(4): 433-448.

Li J, Ehlers T, Sutter J, Varma-O'brien S and Kirchmair J (2007) CAESAR: a new conformer generation algorithm based on recursive buildup and local rotational symmetry consideration. *J Chem Inf Model* **47**(5): 1923-1932.

Lu M, Symersky J, Radchenko M, Koide A, Guo Y, Nie R and Koide S (2013) Structures of a Na$^+$-coupled, substrate-bound MATE multidrug transporter. *Proc Natl Acad Sci U S A* **110**(6): 2099-2104.

Malo C and Berteloot A (1991) Analysis of kinetic data in transport studies: new insights from kinetic studies of Na$^+$-D-glucose cotransport in human intestinal brush-border membrane vesicles using a fast sampling, rapid filtration apparatus. *J Membr Biol* **122**: 127-141.

Martinez-Guerrero LJ and Wright SH (2013) Substrate-dependent inhibition of human MATE1 by cationic ionic liquids. *J Pharmacol Exp Ther* **346**(3): 495-503.

Motohashi h, Nakao Y, Masuda S, Katsura T, Kamba T, Ogawa O and Inui KI (2013) Precise comparison of protein localization among OCT, OAT, and MATE in human kidney. *J Pharm Sci* **102**(9): 3302-3308.

Motohashi h, Sakurai Y, Saito H, Masuda S, Urakami Y, Goto M, Fukatsu A, Ogawa O and Inui

K (2002) Gene expression levels and immunolocalization of organic ion transporters in the

human kidney. *J Am Soc Nephrol* **13**(4): 866-874.

Neuhoff S, Ungell AL, Zamora I and Artursson P (2003) pH-dependent bidirectional transport of

weakly basic drugs across Caco-2 monolayers: implications for drug-drug interactions.

Pharm Res **20**(8): 1141-1148.

Nies AT, Damme K, Schaeffeler E and Schwab M (2012) Multidrug and toxin extrusion proteins

as transporters of antimicrobial drugs. *Expert Opin Drug Metab Toxicol* **8**(12): 1565-1577.

Nies AT, Koepsell H, Damme K and Schwab M (2011) Organic cation transporters (OCTs,

MATEs), in vitro and in vivo evidence for the importance in drug therapy. *Handb Exp*

Pharmacol **201**: 105-167.

Pelis RM and Wright SH (2011) Renal transport of organic anions and cations. *Comprehensive*

Physiol **1**: 1795-1835.

Roos A and Boron WF (1981) Intracellular pH. *Physiol Rev* **61**(2): 296-434.

Roth M, Timmermann BN and Hagenbuch B (2011) Interactions of green tea catechins with

organic anion-transporting polypeptides. *Drug Metab Dispos* **39**(5): 920-926.

Schäli C, Schild L, Overney J and Roch-Ramel F (1983) Secretion of tetraethylammonium by

proximal tubules of rabbit kidneys. *Am J Physiol* **245**: F238-F246.

Schomig E, Lazar A and Grundemann D (2006) Extraneuronal monoamine transporter and

organic cation transporters 1 and 2: a review of transport efficiency. *Handb Exp Pharmacol*

175: 151-180.

Segel IH (1975) *Enzyme Kinetics*. John Wiley & Sons, New York. 957 pp.

Stein WD (1986) *Transport and Diffusion across Cell Membranes*. Academic Press, Inc, New York. 685 pp.

Thevenod F, Ciarimboli G, Leistner M, Wolff NA, Lee WK, Schatz I, Keller T, Al-Monajjed R, Gorboulev V and Koepsell H (2013) Substrate- and cell contact-dependent inhibitor affinity of human organic cation transporter 2: studies with two classical organic cation substrates and the novel substrate Cd^{2+}. *Mol Pharm* **10**(8): 3045-3056.

U.S.Food and Drug A (2012) Preventable Adverse Drug Reactions: A Focus on Drug Interactions.

Volk C, Gorboulev V, Budiman T, Nagel G and Koepsell H (2003) Different affinities of inhibitors to the outwardly and inwardly directed substrate binding site of organic cation transporter 2. *Mol Pharmacol* **64**(5): 1037-1047.

Westholm DE, Salo DR, Viken KJ, Rumbley JN and Anderson GW (2009) The blood-brain barrier thyroxine transporter organic anion-transporting polypeptide 1c1 displays atypical transport kinetics. *Endocrinology* **150**(11): 5153-5162.

Wittwer MB, Zur AA, Khuri N, Kido Y, Kosaka A, Zhang X, Morrissey KM, Sali A, Huang Y and Giacomini KM (2013) Discovery of potent, selective MATE1 inhibitors through prescription drug profiling and computational modeling. *J Med Chem* **56**(3): 781-795.

Wright SH (2014) Multidrug And Toxin Extrusion Proteins, in *Drug Transporters* (You GM, M. E. ed) pp 223-243, Wiley, New Jersey.

Xu Y, Liu X, Wang Y, Zhou N, Peng J, Gong L, Ren J, Luo C, Luo X, Jiang H, Chen K and Zheng M (2015) Combinatorial pharmacophore modeling of Multidrug and Toxin Extrusion Transporter 1 inhibitors: a theoretical perspective for understanding multiple inhibitory mechanisms. *Sci Rep* **5**: 13684.

Yonezawa A, Masuda S, Yokoo S, Katsura T and Inui K (2006) Cisplatin and oxaliplatin, but not

carboplatin and nedaplatin, are substrates for human organic cation transporters (SLC22A1-3

and multidrug and toxin extrusion family). *J Pharmacol Exp Ther* **319**(2): 879-886.

Zhang X, He X, Baker J, Tama F, Chang G and Wright SH (2012) Twelve transmembrane

helices form the functional core of mammalian MATE1 (Multidrug and Toxin Extruder 1)

protein. *J Biol Chem* **287**(33): 27971-27982.

Zhang X, Shirahatti NV, Mahadevan D and Wright SH (2005) A conserved glutamate residue in

transmembrane helix 10 influences substrate specificity of rabbit OCT2 (SLC22A2). *J Biol

Chem* **280**(41): 34813-34822.

Footnotes

Portions of this work were a part of a dissertation that was submitted by Dr. Martinez-Guerrero to the University of Arizona in accordance with academic requirements.

Figure Legends

Figure 1. 2D Structures of the four MATE substrates used in this study: MPP, NBD-MTMA, cimetidine and metformin. The Tanimoto similarity coefficients were calculated using Discovery Studio.

Figure 2. Time course of MATE1-mediated transport (expressed as clearance; $\mu l\ cm^{-2}$) of [^{3}H]cimetidine (~10 nM), [^{3}H]MPP (~10 nM), [^{14}C]metformin (~10 μM), and [^{3}H]NBD-MTMA (~10 nM). Each point is the mean (±SE) of uptakes determined in 5 replicate wells (corrected for transport measured in mild type CHO cells), all determined in a single, representative experiment.

Figure 3. Kinetics of MATE1-mediated transport of (A) MPP, (B) NBD-MTMA, (C) cimetidine, and (D) metformin. Kinetic values were based on the inhibition of radiolabeled substrate resulting from exposure to increasing concentration of unlabeled substrate. Each point is the mean (±SE) of 30 sec uptakes determined in two separate experiments with each substrate (n=2), each of which was based on uptakes measured in six replicate wells. The line was fit to equation 1 using Prism (GraphPad; St. Louis, MO)

Figure 4. Kinetics of interaction of the four test substrates with one another. The uptake of each of the radiolabeled substrates (A, [^{3}H]MPP, ~10 nM; B, [^{3}H]NBD-MTMA, ~10 nM; C, [^{3}H]cimetidine, ~10 nM; D, [^{14}C]metformin, ~10 μM) was measured in the presence of increasing concentrations of the unlabeled test substrates. Each point is the mean (±SE) of 30 sec uptakes determined in two separate experiments with each substrate (n=2), each of which

was based on uptakes measured in six replicate wells; uptakes normalized to that measured in the absence of inhibitor. The line was fit to equation 2 using Prism (GraphPad; St. Louis, MO). The table lists the IC_{50} values (±SE; n=2) for each substrate/inhibitor pair; the grey shaded boxes list the K_{tapp} values for MATE1-mediated transport of each substrate (taken from Fig. 3).

Figure 5. Inhibition of test substrate uptake produced by 50 µM concentrations of each of 400 test inhibitors from the NIH Clinical Collection. Each horizontal grey bar represents the mean (±SE) of 30 sec substrate uptakes (A, [^{3}H]MPP, ~10 nM; B, [^{3}H]NBD-MTMA, ~10 nM; C, [^{3}H]cimetidine, ~10 nM; D, [^{14}C]metformin, ~10 µM) measured in the presence of 50 µM inhibitor, expressed of a percentage of uptake measured in the absence of inhibitor; determined in two experiments (n=2), each of which was performed in triplicate (all uptakes corrected for substrate accumulation measured in duplicate in wild type CHO cells. The rank order of inhibitors, from least effective (at the top) to most effective (at the bottom) is the same for all four test substrates. Red dashed lines represent control (100%) uptake; red dotted lines indicate 50% inhibition of control uptake.

Figure 6. Pairwise comparison of inhibition of MATE1-mediated transport of each substrate by the test compounds of the NCC (data from Fig. 5). Dashed blue lines represent equivalent inhibition of the compared substrates; the solid line red lines represent simple linear regressions of the data.

Figure 7. Kinetics of inhibition of the MATE1-mediated transport of four test substrates (A, [^{3}H]MPP, ~10 nM; B, [^{3}H]NBD-MTMA, ~10 nM; C, [^{3}H]cimetidine, ~10 nM; D,

[^{14}C]metformin, ~10 µM) exposed to increasing concentrations of five test inhibitors. Each point

is the mean (±SE) of 30 sec uptakes determined in two separate experiments with each substrate

(n=2), each of which was based on uptakes measured in six replicate wells; uptakes normalized

to that measured in the absence of inhibitor. The line was fit to equation 2 using Prism

(GraphPad; St. Louis, MO).

Figure 8. Pairwise comparison of log IC$_{50}$ values for inhibition of MATE1-mediated transport of

each substrate by 22 compounds selected from the NCC, plus the IC$_{50}$ values for inhibition of

each substrate produced by the four test substrates. Dashed lines represent equivalent inhibition

of the compared substrates; the solid line represents a simple linear regression of the data.

Figure 9. Common feature pharmacophores of MATE1 inhibitors. The pharmacophores were

based on IC$_{50}$ values of 22 test drugs from the NCC plus the four test substrates when used as

inhibitors of MATE-mediated transport of each labeled substrate (A, MPP; B, NBD-MTMA; C,

cimetidine; D, metformin). Each is shown overlaid with the structure of gabexate (IC$_{50}$ values of

0.6 – 0.7 µM). Pharmacophore features are one ionizable (red; cationic) feature; one hydrophobe

(cyan; two for metformin), two hydrogen bond acceptors (green; one for metformin). (E) Spatial

alignment of the four pharmacophores.

Figure 10. The relationship between measured and predicted IC$_{50}$ values based on the models

shown in Figure 9. The dashed line represents identity between measured and predicted. Data

points shown as circles represent the 26 compounds that comprised the training set for model

development; the six points shown as green hexagons represent six test set compounds and their

predicted vs. measured values for inhibition of MPP transport (see Table S1). For clarity the

individual regression lines (log measured vs. log predicted) for the four substrates are not shown,

but the r values for these lines were: MPP, 0.80; NBD-MTMA, 0.81; cimetidine, 0.81,

metformin, 0.79.

Table 1. Kinetics of MATE1-mediated transport of four structurally distinct substrates.

Substrate	K_{tapp} (μM)	J_{max} (pmol cm^{-2} min^{-1})	J_{max}/K_{tapp} (Transport Efficiency) (x10^{-3} cm/min)
MPP	34.5 ± 12.9	83.2 ± 29.3	2.4
NBD-MTMA	105 ± 39.8	56.2 ± 20.3	0.5
Metformin	336 ± 202	344 ± 181	1.0
Cimetidine	2.2 ± 0.8	4.9 ± 1.7	2.2

Table 2. Kinetics of inhibition (reported as IC_{50}s) of MATE1-mediated transport of four structurally distinct substrates produced by 22 compounds selected from the National Clinical Collection. The values shown in shaded boxes represent measured apparent K_t values for the transport of the indicated substrate, rather than IC_{50}s.

	Substrate			
	MPP	NBD-MTMA	Cimetidine	Metformin
Inhibitors	IC_{50} or K_{tapp} (μM)			
MPP	34.5 ± 12.9	105.5 ± 8.2	42.3 ± 0.4	26.3 ± 0.4
NBD-MTMA	91.6 ± 0.5	105 ± 39.8	73.4 ± 0.3	50.5 ± 3.2
Cimetidine	0.92 ± 0.02	1.09 ± 0.21	2.2 ± 0.8	0.62 ± 0.07
Metformin	767 ± 11.6	1085 ± 25	372 ± 4.1	336 ± 202
Famotidine	0.28 ± 0.05	1.66 ± 0.8	0.48 ± 0.06	0.27 ± 0.03
Gabexate	0.70 ± 0.09	0.72 ± 0.14	0.56 ± 0.09	0.58 ± 0.14
Donepezil	1.22 ± 0.17	1.47 ± 0.19	1.27 ± 0.06	0.78 ± 0.13
Trimethoprim	1.40 ± 0.14	1.45 ± 0.19	1.61 ± 0.12	0.75 ± 0.07
Prochlorperazine	10.6 ± 1.8	14.1 ± 6.3	15.3 ± 2.20	7.89 ± 0.80
Nafadotride	11.5 ± 1.01	10.4 ± 2.02	19.9 ± 1.39	7.3 ± 0.57
Ranitidine	13.4 ± 1.18	13.1 ± 3.50	22.3 ± 2.99	11.0 ± 1.20
Esmolol	16.2 ± 0.89	24.5 ± 2.88	12.7 ± 1.64	11.0 ± 0.98
Omeprazole	19.8 ± 2.91	17.2 ± 2.74	23.5 ± 2.48	16.1 ± 1.14
Ketotifen	22.3 ± 3.08	24.3 ± 2.55	27.0 ± 1.68	12.7 ± 1.27
Fluperlapine	37.1 ± 5.7	53.4 ± 14.5	41.2 ± 6.08	32.6 ± 4.92
Vesamicol	49.8 ± 8.9	74.6 ± 20.0	83.8 ± 23.0	39.3 ± 7.00
Cortisone	56.9 ± 6.47	77.4 ± 11.2	131 ± 13.3	28.5 ± 2.79
Hydrocortisone	66.7 ± 7.42	57.3 ± 11.7	110 ± 18.2	64.1 ± 9.2
Levofloxacin	71.5 ± 10.5	35.0 ± 9.88	90.5 ± 10.9	45.8 ± 2.91
Tryptoline	103 ± 10.4	142.6 ± 27.5	110 ± 13.6	95.6 ± 11.7
Rolipram	147 ± 12.9	183 ± 40.8	111 ± 11.4	124 ± 11.0
Stiripentol	201 ± 28.7	194 ± 79.5	331 ± 84.3	170 ± 49.8
Cerivistatin	249 ± 55.9	170 ± 47.3	204 ± 58.6	241 ± 50.4
Venlafaxine	366 ± 55.0	332 ± 34.4	303 ± 33.6	168 ± 25.8
Ticlopidine	678 ± 98.3	444 ± 67.3	692 ± 110	442 ± 56.1
5-Fluoro-2-pyrimidone	1444 ± 315	1587 ± 384	N/D	5138 ± 2114

N/D not determined

Figure 1

Figure 2

A.

B.

C.

D.
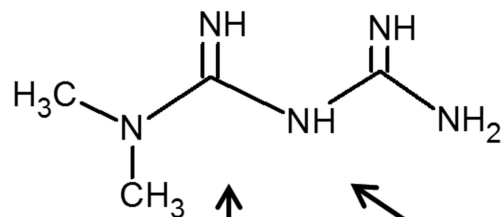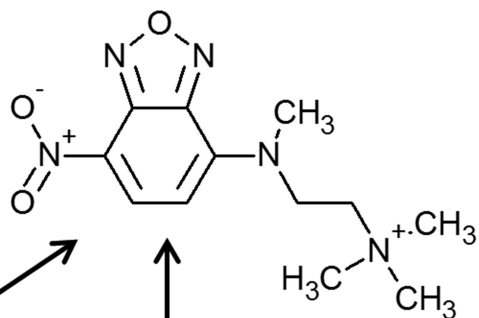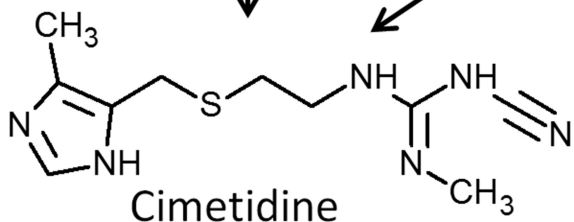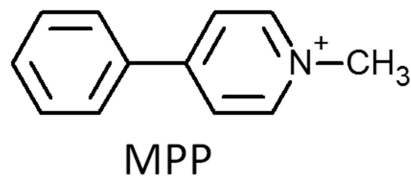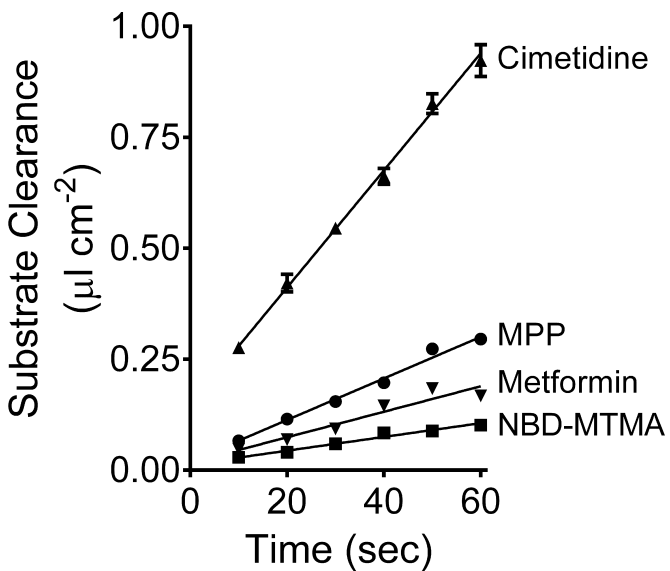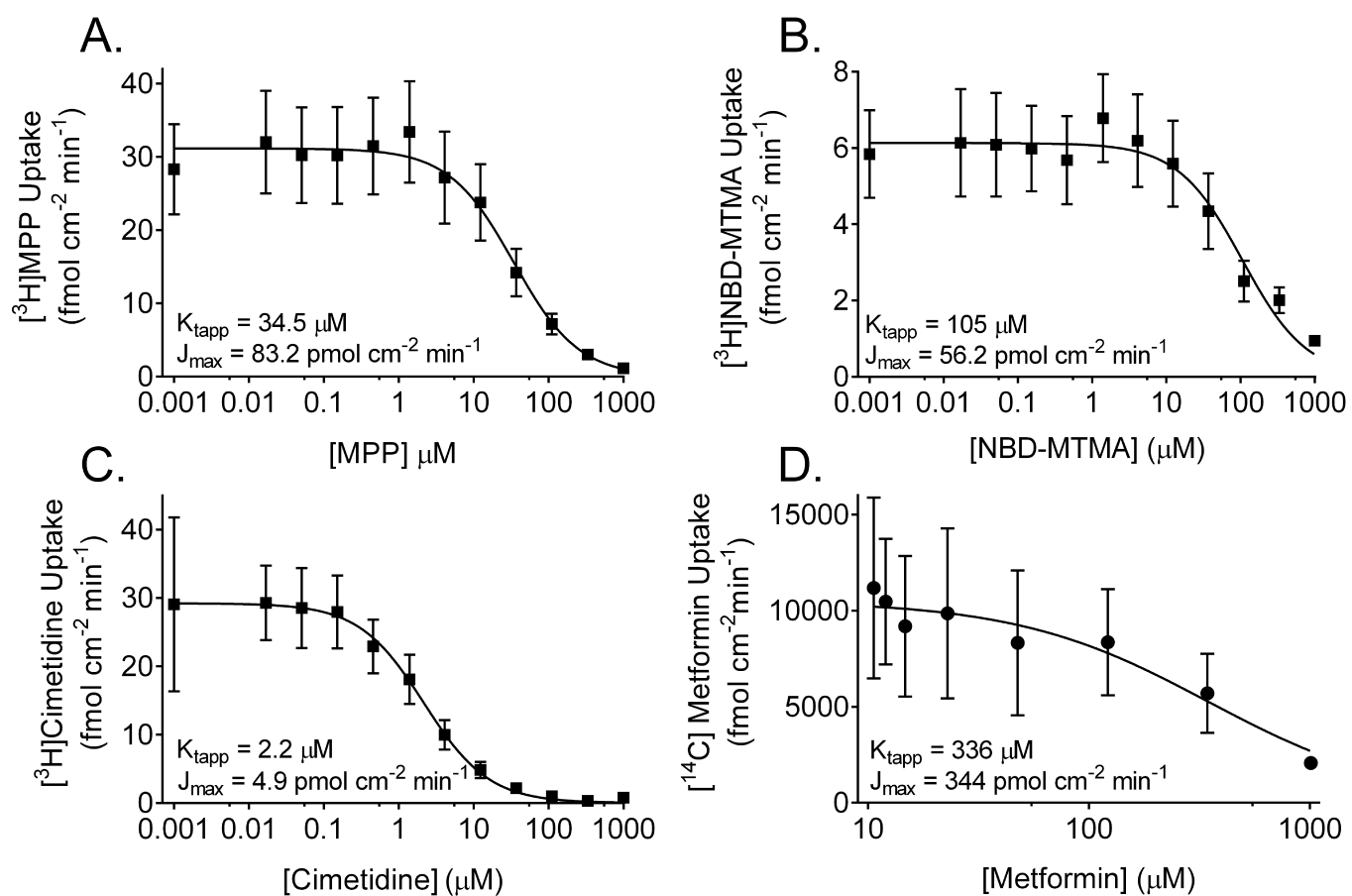
Figure 3

	SUBSTRATE			
	MPP	NBD-MTMA	Cimetidine	Metformin
Inhibitors	IC_{50} or K_{tapp} (µM)			
mpp	**34.5 ± 12.9**	105.5 ± 8.2	42.3 ± 0.4	26.3 ± 0.4
nbd-mtma	91.6 ± 0.5	**105 ± 39.8**	73.4 ± 0.3	50.5 ± 3.2
cimetidine	0.92 ± 0.02	1.09 ± 0.21	**2.2 ± 0.8**	0.62 ± 0.07
metformin	767 ± 11.6	1085 ± 25	372 ± 4.1	**336 ± 202**

Figure 4
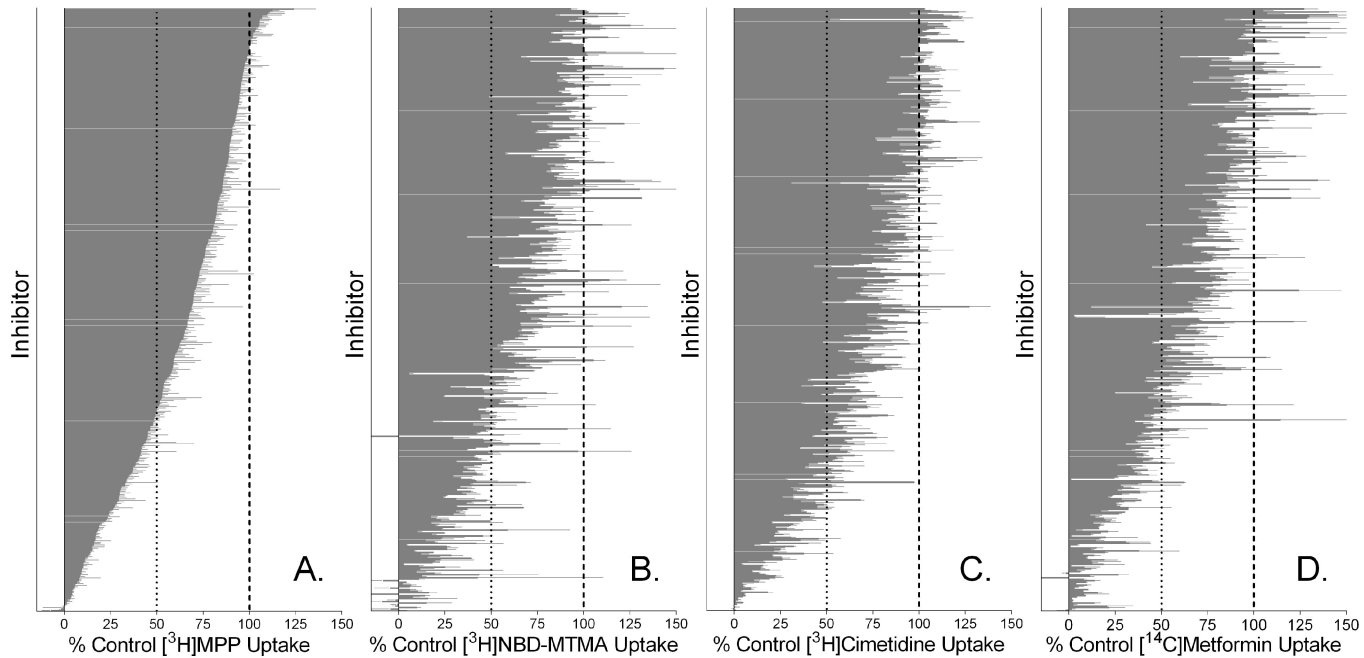
Figure 5
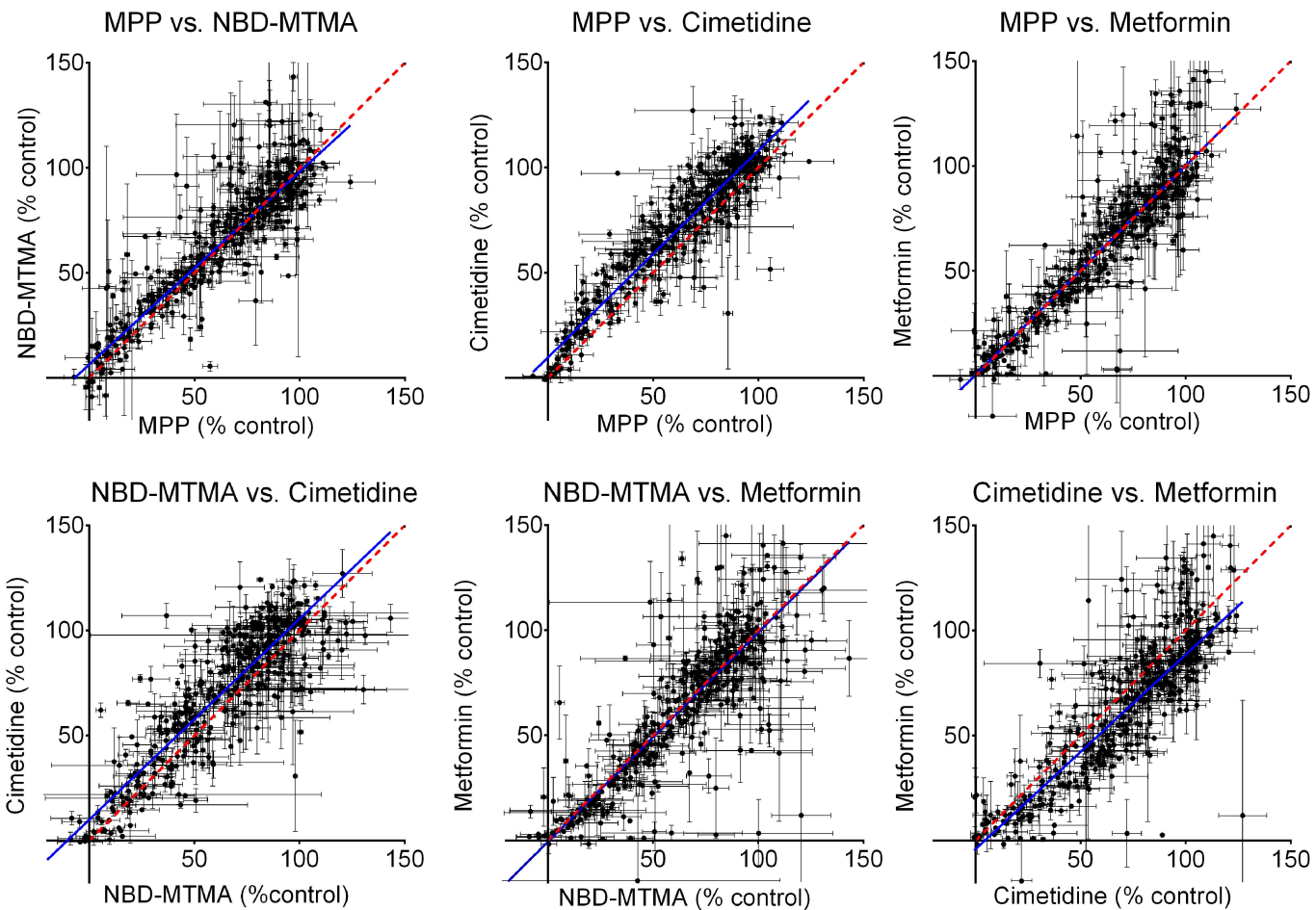
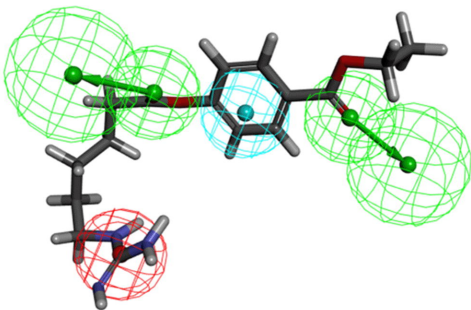Figure 6
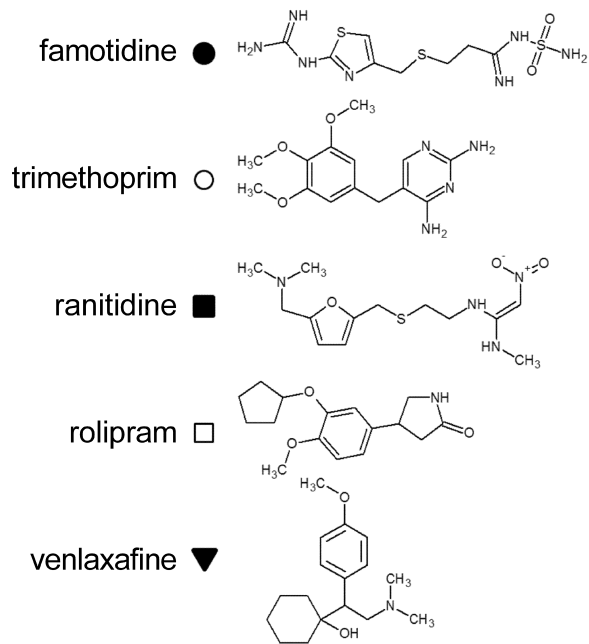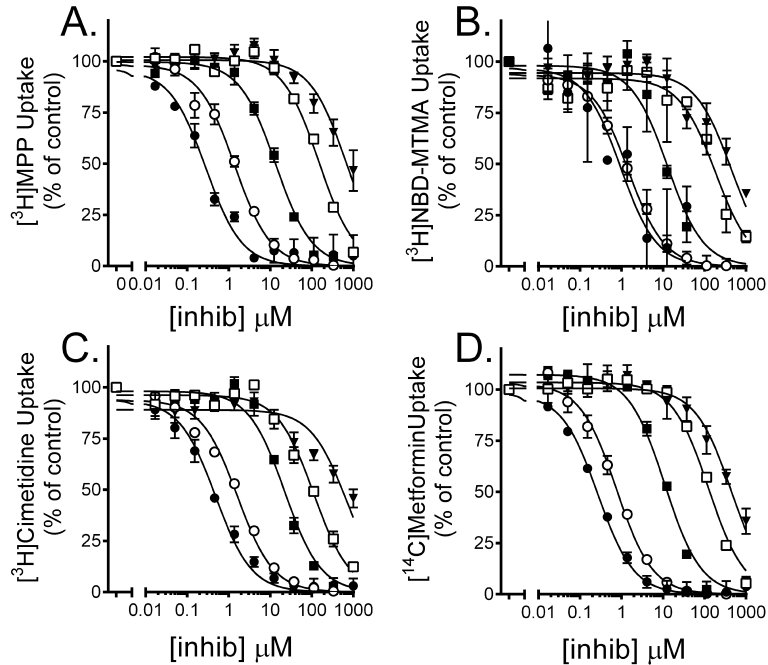
Figure 7
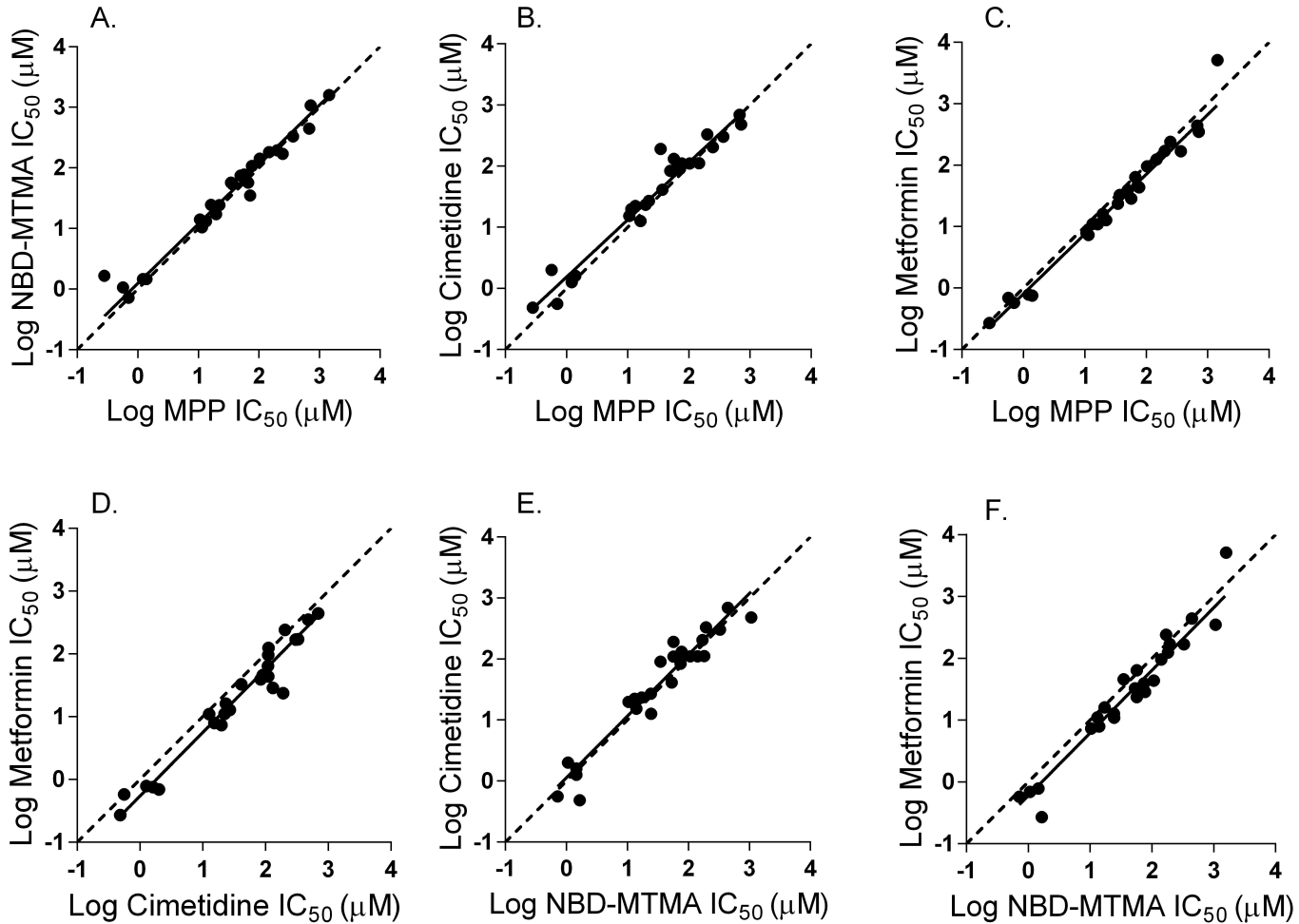
Figure 8

A.   *vs. MPP*
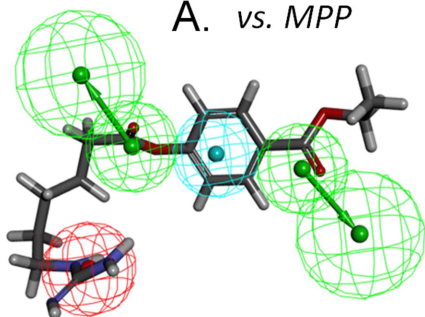
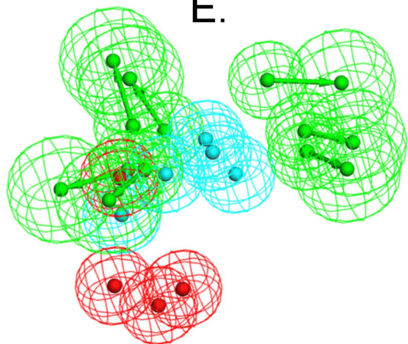B.   *vs. NBD-MTMA*
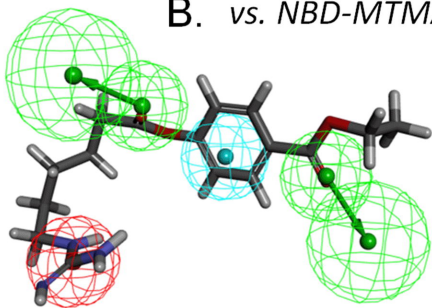
C.   *vs. cimetidine*
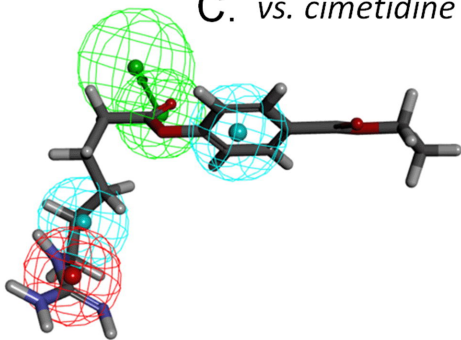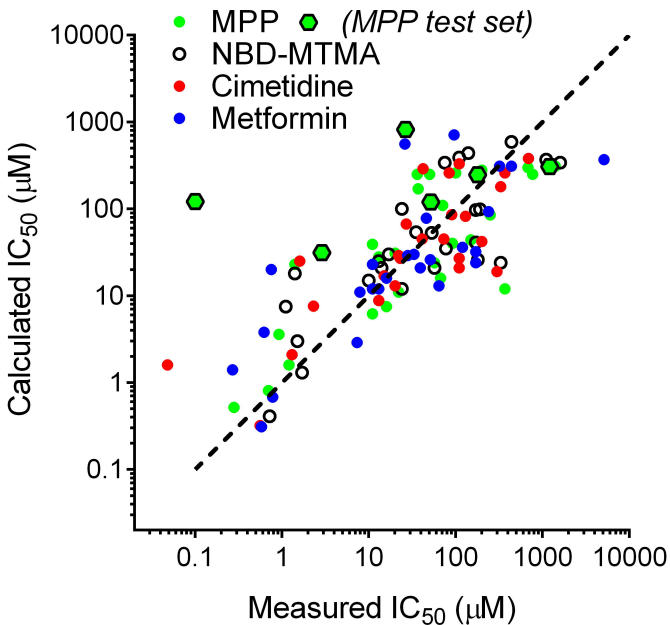
D.   *vs. metformin*

E.

Figure 9

Figure 10